Surfactant-Encapsulated Europium-Substituted Heteropolyoxotungatate: The Structural Characterization and Photophysical Properties of Its Solid State, Solvent-Casting Film, and Langmuir−Blodgett Film

Weifeng Bu,[†,‡] Lixin Wu,*[,‡] Xi Zhang,[‡] and Au-Chin Tang[†]

State Key Laboratory for Theoretical and Computational Chemistry, Jilin University, Changchun 130023, Jilin, People's Republic of China, and Key Laboratory for Supramolecular Structure and Materials of Ministry of Education, Jilin University, Changchun 130023, Jilin, People's Republic of China

Received: June 10, 2003; In Final Form: September 30, 2003

The surfactant-encapsulated europium-substituted heteropolyoxotungatate, $(DODA)_{11}H_2[Eu(SiW_{11}O_{39})_2(H_2O)_4]$ (SEC-2), is structurally characterized in detail and its photophysical behaviors are investigated. The DODA alkyl chains of SEC-2 are well ordered in the solid state, solvent-casting film, and Langmuir−Blodgett (LB) film. The europium-substituted heteropolyoxotungatate (POM-2a) is organized in the solvent-casting and LB films. A comparison of the intensities of the $W-O_d$ antisymmetrical stretching band between the infrared transmission and reflection absorption spectra of the LB films suggests that the long axis direction of POM-2a is parallel to the substrates. The solid-state SEC-2 shows two different lamellar structures with interlayer distances of 3.6 and 4.9 nm, respectively. The layer structures are well defined in both the solvent-casting and LB films and have lamellar distances of 3.6 and 4.9 nm, respectively. In short periodicities, it is considered that the alkyl chains are partially interdigitated, and the interdigitated length may reach 1.3 nm. SEC-2 exhibits the characteristic $^5D_0 \rightarrow {}^7F_j$ ($j = 0-4$) Eu^{3+} emission. The bands in both the excitation and emission spectra of $K_{13}Eu(SiW_{11}O_{39})_2 \cdot 20H_2O$ (POM-2) and SEC-2 solutions (1 mM) show different intensities because of their various chemical microenvironments. The strong oxygen-to-tungsten charge transfer (O→W LMCT) bands of POM-2a appear in the excitation spectra of the solvent-casting and LB films, indicating an efficient intramolecular energy transfer from the O→W LMCT states to Eu^{3+} ions. The luminescent lifetimes of SEC-2 are much shorter than those of the naked POM-2 because of the coordinated water molecules to Eu^{3+} in SEC-2. The solution, solid state, solvent-casting films, and LB films of SEC-2 display their different photophysical properties such as spectrum, lifetime, and energy transfer from the O→W LMCT states to Eu^{3+} ions. The photophysical behaviors of Eu−POMs can be modified by their organizational structures, which are significant for the future realizations of functional devices.

Introduction

The device realization of functional materials requires oriented incorporations of functional units into ordered thin film. One of the promising ways for this goal is the artificial incorporation of these functional units into amphiphilic matrixes, where they can be organized through solvent-casting or Langmuir−Blodgett (LB) techniques.[1,2] Polyoxometalates (POMs) are intriguing building blocks in the fabrication of functional materials because they possess both a well-defined molecular weight and a structural topology, and furthermore, display rich and interesting magnetic, electronic, medical, photophysical, and catalytic properties.[3,4] Langmuir monolayers of dimethyl dioctadecylammonium (DODA) amphiphiles can adsorb POMs from an aqueous subphase at the air/water interface through electrostatic interaction.[5−9] LB films prepared through transferring those layers onto solid substrates present magnetic[6,7] and luminescent[8,9] properties. The cationic surfactants can replace the counterions of POMs, forming the surfactant-encapsulated clusters (SECs).[10−16] SECs possess a hydrophobic DODA shell and an encapsulated hydrophilic POM core with a well-defined composition. The encapsulated clusters are soluble in nonpolar solvents such as chloroform, benzene, or toluene. The dendron-encapsulated POMs aim at rapidly prototypical smart catalyst (dendrizymes), which are structurally related to those natural metalloproteins.[17] Well-ordered thin films of SECs are readily prepared by LB technique and solvent-casting method. These supramolecular assemblies, therefore, are offering promising approaches toward new soft materials containing POMs.

When DODA molecules enwrap different POMs, these organic/inorganic complexes demonstrate various packing structures. The structure of solvent-casting films of SECs is influenced by evaporation rates of organic solvents. When the solvent-casting films are prepared through slow evaporation of chloroform, the alkyl chains in $(DODA)_{16}As_4W_{30}Cu_4O_{112}$ (SEC-1) are believed to possess a partial interdigitatation, and the interdigitated length may reach 1.6 nm.[14] Its LB multilayer films possess a translational distance of 5.1 nm, and the long-axis of the POM is parallel to the substrate in the matrix of DODA.[15] However, previous studies were mainly concentrated on structural characterizations of thin films and solution of SECs.

A europium-substituted heteropolyoxotungatate cluster, $K_{13}Eu(SiW_{11}O_{39})_2 \cdot 20H_2O$ (POM-2), shows the characteristic $^5D_0 \rightarrow {}^7F_j$ ($j = 0-4$) transitions of Eu^{3+} emission. Its broad oxygen-to-tungsten charge transfer (O→W, LMCT) bands illustrate strong temperature dependence. That is to say, they

* To whom correspondence should be addressed. Fax: +86 431-8980729; e-mail: wulx@jlu.edu.cn.
† State Key Laboratory for Theoretical and Computational Chemistry.
‡ Key Laboratory for Supramolecular Structure and Materials of Ministry of Education.

10.1021/jp0356416 CCC: $25.00
Published on Web 11/05/2003

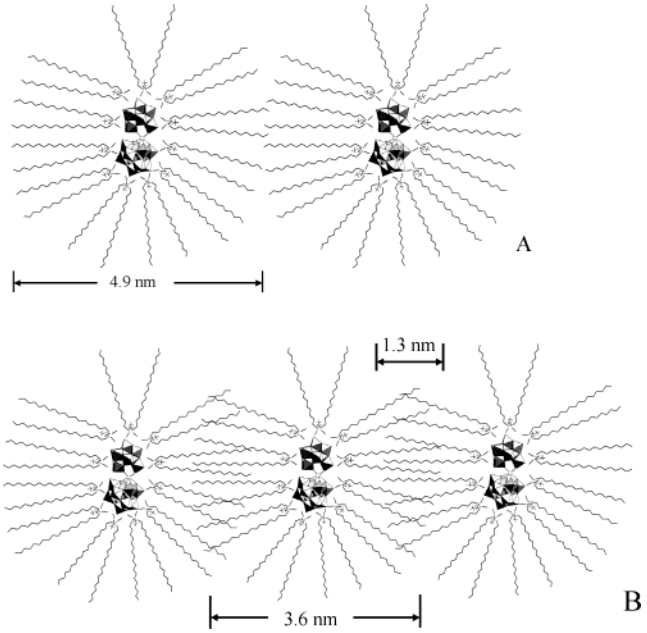

Figure 1. The schematic drawing of chemical structure of SEC-2 that shows a core−shell structure, (A) monolayer and (B) interdigitation model.

cannot be detected at room temperature but at low temperature. This is associated with the competition between the thermal relaxation of the O→W LMCT states and the energy transfer to Eu^{3+}.[18,19] In $Eu(SiW_{11}O_{39})_2^{13-}$, POM-2a, Eu^{3+} ion is coordinated by two lacunary Keggin-type $SiW_{11}O_{39}^{8-}$ groups through eight oxygen atoms and forms an Archimededian antiprism.[20] The polytungstate groups consisting of distorted tungstate octahedra have approximate C_{4v} (actual C_s) symmetry.[18] Herein, we prepared an organic/inorganic composite, $(DODA)_{11}H_2[Eu(SiW_{11}O_{39})_2(H_2O)_4]$ (SEC-2), bearing a core−shell ellipsoid as schematically drawn in Figure 1, and conducted a comprehensive investigation of SEC-2 on both its structures and photophysical behaviors. Since the photophysical behaviors of Eu^{3+} are sensitive to its environments,[21] different organized structures for POM-2a show various photophysical behaviors. The aim of this work is to demonstrate that, through controlling the organizational structures of Eu−POM based materials by solvent-casting and LB film techniques, we are able to control the photophysical properties of the materials fabricated therein. These results are significant for the realization of Eu−POM based electroluminescent devices.

Experimental Section

Preparation of SEC-2. POM-2 was freshly prepared according to the literature procedures.[22] Dimethyl dioctadecylammonium bromide (DODA·Br, 99%) was purchased from Acros Organics and used as received. SEC-2 was synthesized using the previously reported procedures.[11−16] POM-2 was dissolved in aqueous solution (pH = 6), and then chloroform solution of DODA·Br was added with stirring. The initial molar ratio of DODA·Br to POM-2 was controlled at 11:1. The organic phase was separated and SEC-2 was obtained by evaporating the chloroform to dryness. Then, the sample was further dried in a vacuum until its weight remained constant. ^{1}H NMR ($CDCl_3$, 500 MHz) δ: 0.88 (t, J = 7.5 Hz, 6H, CH_3), 1.24 (m, 60H, CH_2), 1.59 (br, 4H, CH_2), 3.22 (br, 10H, NCH_2, and NCH_3). IR (KBr, cm^{-1}): ν = 3469, 2955, 2919, 2849, 1635, 1484, 1468, 1379, 998, 944, 890, 816, 772, 721, 545, 524, 475. Anal. Calc. for SEC-2 ($C_{418}H_{890}N_{11}O_{82}W_{22}Si_2Eu$, 11636.54): C, 43.14; H, 7.71; N, 1.32. Found: C, 43.55; H, 8.07; N, 1.27. Therefore, this new polyoxometalate-based compound should correspond to a tentative formula: $(DODA)_{11}H_2[Eu(SiW_{11}O_{39})_2(H_2O)_4]$.

Solvent-Casting and Langmuir−Blodgett Films. The chloroform solution of SEC-2 with a concentration of 1.95 mg/mL was directly cast onto a quartz substrate for wide-angle X-ray diffraction measurement and a CaF_2 (1 × 2 cm^2) wafer for Fourier transform infrared (FT-IR) measurements. All casting films were prepared under air for natural evaporation of chloroform (20 min) and then dried in vacuum desiccators at room temperature to remove the residual solvent. The mean thickness was estimated to be 250−300 nm by comparing the IR absorbance of the alkyl chains in the solvent-casting and LB films of SEC-2.

The surface pressure−area (π−A) isotherms of SEC-2 were carried out on a Nima 622D Langmuir trough (double troughs) with a Wilhelmy plate balance at a constant barrier rate of 20 cm^2/min. Thirty-microliter chloroform solution (1.95 mg/mL) of SEC-2 was spread onto a distilled deionized water subphase with a pH value of 5.7 and a temperature of 18 °C. After evaporation of the solvent, the monolayers were compressed up to a surface pressure of 20 mN/m. The Langmuir monolayers were then allowed to equilibrate for 30 min at this pressure, and the condensed monolayers were finally transferred by the vertical dipping method onto CaF_2 substrates for IR and polarized IR measurements, onto gold substrates for IR reflection absorption (RA) measurement, onto quartz substrates for wide-angle X-ray diffraction, and UV−vis absorption measurements. In all cases, the dipping rate for the transfer of LB films was set at 0.6 cm/min.

Spectroscopic Measurements. FT-IR measurements were performed on a Bruker IFS66V FT-IR spectrometer equipped with a DGTS detector for the solid-state SEC-2 (32 scans) and an MCT detector for the solvent-casting and LB films (1024 scans), respectively. The spectra were recorded with a resolution 4 cm^{-1}. The polarized IR measurements were conducted with an incident angle of 0° and 60°, respectively, together with a polarizer. The IR−RA spectrum was measured with an incidence angle of 80°. UV−vis absorption spectra of the LB films of SEC-2 were recorded on a Shimadzu UV-3100 spectrometer and the slit width was set at 2 nm. Luminescent measurements were performed on a Spex FL=2T2 spectrophotometer using a xenon lamp as the excitation source. The luminescent lifetimes were recorded on a Spex 1934D-phosphorescence spectrophotometer. The luminescent spectra of the solutions of POM-2 and SEC-2 were recorded at the identical conditions such as concentrations and slit widths so that the intensities of the excitation and emission bands are comparable. Solid sample, solvent-casting films, and multilayer LB films of SEC-2 were characterized by wide-angle X-ray diffraction, which were carried out on a Rigaku X-ray diffractometer (D/max rA, using Cu K_α radiation of a wavelength of 1.542 Å). All spectroscopic measurements were done at room temperature.

Results and Discussion

Characterization for SEC-2. SEC-2 is immiscible in water but readily dissolves in organic media such as benzene, toluene, or chloroform. In contrast, POM-2 is only soluble in water. This indicates that POM-2a has been successfully encapsulated with DODA·Br. This complex is stable in air, and no structural changes of POM-2a seem to take place on water subphase according to the identical IR and UV−vis spectra of POM-2 and SEC-2. Thermogravimetric analysis at the range of 30−

160 °C shows that there is no crystal water in SEC-2. However, its IR absorption bands at 3468 and 1635 cm^{-1}, because of OH stretching and scissoring modes, respectively, strongly suggest the presence of water molecules. This should result from the coordinated water to Eu^{3+}, which leads to much shorter lifetimes of SEC-2. Therefore, combining the element and thermogravimetric analysis, SEC-2 should correspond to the following formula: $(DODA)_{11}H_2[Eu(SiW_{11}O_{39})_2(H_2O)_4]$.

^1H NMR spectra of SEC-2 confirm the presence of surfactants in the encapsulated cluster. In contrast to those of DODA·Br alone, the resonance signals of DODA in SEC-2 changed as follows. (1) The signal of *N*-methyl proton is significantly broadened and shifted to high field by δ 0.18. (2) The proton signal of *N*-methylene, which should be split into a triplet, shows up as a considerably broadened singlet and shifts toward high field by δ 0.29. The peak broadening and shifting should result from the strong electrostatic interaction between surfactants and POM-2a. That is, the surfactants are immobilized on the surface of POM-2a in organic phase, and to some extent, their mobility is confined, especially for their head parts. The shift and broadening of the resonance signals of SEC-2 are different from those in the literature,[11,13,16] attributed to the different POMs used in the SECs. ^{183}W NMR measurements for SEC-2 in $CDCl_3$ failed. Similar results are also observed by Pope et al., which was thought to be due to the solution's high viscosity and consequently lower mobility of POM-2a.[23]

In the IR spectrum of the solid-state SEC-2, bands at 2919 and 2849 cm^{-1} are assigned to CH_2 antisymmetric and symmetric stretching modes of DODA alkyl chains of SEC-2, respectively, which are consistent with those of crystalline DODA·Br (2918 and 2850 cm^{-1}). The frequencies of the CH_2 stretching bands are sensitive to the conformation of a hydrocarbon chain; low frequencies (2918 and 2848 cm^{-1}) of the bands are characteristic of a highly ordered alkyl chain, while their upward shifts (2927 and 2856 cm^{-1}) are indicative of the increase in conformational disorder, that is, gauche conformers, in the hydrocarbon chain.[24−27] The fact that the CH_2 stretching bands appear at 2919 and 2949 cm^{-1} in the infrared spectrum suggests that the DODA alkyl chains are well-ordered in the solid-state SEC-2. However, this does not mean the alkyl chains are in a fully extended conformation. POM-2a consists of two lacunary Keggin structures of $SiW_{11}O_{39}^{8-}$ linked by a europium ion.[19] Considering the radius (0.52 nm)[28] of Keggin-type POMs, the surface area of POM-2a should be around 6.8 nm^2. Thus, every DODA will occupy an area of 0.62 nm^2, which is similar to the lateral area (0.567 nm^2) in the crystal structure of DODA·Br.[29] X-ray analysis of crystalline DODA·Br represents that one of its two hydrocarbon chains is bent at an almost right angle in the third carbon atom, while after that carbon, both chains have a trans-zigzag conformation with their molecular planes parallel to each other. On the basis of their similar lateral areas and IR frequencies, the conformation of DODA in SEC-2 is similar to that of crystalline DODA·Br. The peaks at 2956 and 1379 cm^{-1} should be attributed to CH_3 antisymmetric stretching and deformation modes, respectively. The band at 1468 cm^{-1} is assigned to a CH_2 scissoring mode. The shoulder peaks at 1484 cm^{-1} may result from the interaction of the CH_2 groups with N^+, which leads to a change of charge distribution of the α-carbon atom of SEC-2.[30,31] Strong bands are observed below 1000 cm^{-1} for POM-2a vibrations.[28] The detailed assignments are summarized in Table 1.

Further evidence for the conformational order of DODAs comes from X-ray diffraction of the solid-state SEC-2. Figure 2A (inset) represents a Bragg peak at 21.4°, corresponding to a

TABLE 1: The Assignments of Infrared Spectra of SEC-2 in Its Solid State, Solvent-Casting Film, and LB Film[b]

KBr (cm^{-1})	casting films (cm^{-1})	LB films (cm^{-1})	assignments[a]
3469	3471	3470	O−H antisym. str.
2919	2920	2918	C−H antisym. str.
2849	2850	2850	C−H sym. str.
1635	1635	1635	O−H scissoring
1484	1484	1484	CH_2N scissoring
1468	1468	1468	CH_2 scissoring
1379	1379	1379	CH_3 scissoring
998	992	995	
944	947	947, 950	$W-O_d$ antisym. str.
		910	$Si-O_a$ antisym. str.
890	897	897	$W-O_b-W$ antisym. str.
		870	$W-O_b-W$ antisym. str.
		860	$W-O_b-W$ antisym. str.
816	847	812	$W-O_c-W$ antisym. str.
772	832		$W-O_c-W$ antisym. str.

[a] Antisym. str., antisymmetrical stretching; sym. str., symmetrical stretching. [b] According to refs 5 and 28.

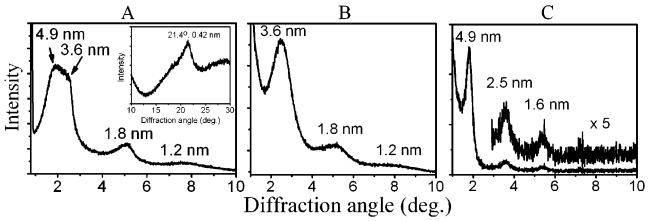

Figure 2. X-ray diffraction pattern of SEC-2 in the low angle region at its solid state (inset: X-ray diffraction pattern in high angle region) (A), the solvent-casting films (B), and a nineteen-layer LB film (C).

spacing of 0.42 nm, which agrees well with the lateral packing of DODA·Br in its crystal structure.[29] The X-ray diffraction pattern (Figure 2A) shows four Bragg diffraction peaks at 1.81, 2.46, 4.96, and 7.48°, corresponding to the spacings of 4.9, 3.6, 1.8, and 1.2 nm, respectively. The ratio of the latter three spacings suggests that the signals arise from a lamellar structure with a layer distance of 3.6 nm. POM-2a is a peanut-shaped POM with a long-to-short axis ratio of 2:1; thus, most of DODAs are proposed to align along its long axis as shown in Figure 1A.[14,15] Crystalline DODA·Br possesses a lamellar structure with an interlayer distance of 3.811 nm.[29] Taking the short-axis diameter of POM-2a and the length of DODA into account, the total thickness of a single SEC-2 should be around 4.8 nm, which is consistent with the first spacing in the X-ray diffraction of the solid-state SEC-2. The short layer distance should be attributed to the partially interdigitated DODA alkyl chains in the solid-state SEC-2, and the interdigitated depth is estimated to be 1.3 nm (Figure 1B). The two different periodicities will be further supported by the luminescent lifetimes of the solid-state SEC-2.

Solvent-Casting Films. The CH_2 stretching bands appear at 2920 and 2950 cm^{-1} in the infrared spectrum of the solvent-casting film of SEC-2 (Table 1), indicative of well-ordered DODA alkyl chains. A powerful method to determine the orientation of molecules in thin films is linear dichroism of infrared spectroscopy.[32] The in-plane dichroic ratio, α, can be defined for a particular IR peak by the relation, $\alpha = A_\perp/A_\parallel$, where $A_\perp$ and $A_\parallel$ are the absorbance of the thin films when the light polarization angles are set at 90° and 0°, respectively. The out-of-plane IR linear dichromism is represented by the usual dichroic ratio β: $\beta = A_\parallel(i = 60°)/A_\parallel(i = 0°)$, where $A(i)$ is the absorption coefficient and i denotes the angle between the planes of LB film and the IR light electric vector. This ratio β allows one to evaluate the angle between the normal of the substrate

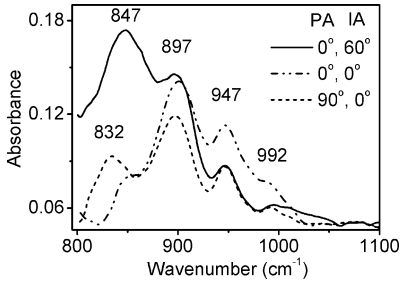

Figure 3. Polarized infrared spectra of the solvent-casting films of SEC-2. The angle between the plane of the substrate and the electric field is either 0° or 60°, the polarized angle is set to 0° or 90°. PA: polarized angle, IA: incident angle.

TABLE 2: The Infrared Linear Dichromic Ratios of the Dipole Moments of SEC-2 in Its Casting and LB Films[a]

	casting films		LB films	
wavenumber (cm^{-1})	α	β	α	β
947 ν W−O_d antisym. str.	1.02	0.64	1.14	1.45
897 ν W−O_b−W antisym. str.	0.98	0.47	0.58	0.45
847 ν W−O_c−W antisym. str.	0	12.53		

[a] α = in-plane dichromic ratio; β = out-of-plane dichromic ratio.

and the dipole moment of particular vibration with a precision of 5°.[5] Here, we estimate the average tilt angle of DODA alkyl chains to be about 30° in the solvent-casting films of SEC-2. Considering the shape of POM-2a, the distribution of the DODA alkyl chains should not be completely global, but anisotropic, which easily leads to a specific orientation of the alkyl chains in the solvent-casting film of SEC-2.

As demonstrated in Figure 3, pronounced in-plane and out-of-plane dichromisms have been observed for the absorption bands of POM-2a in the solvent-casting film of SEC-2. Their dichromic ratios are summarized in Table 2. When the polarized angle is set at 90° and the incident angle is 0°, a band at 847 cm^{-1} due to a W−O_c−W antisymmetric stretching mode disappears, and a new band at 837 cm^{-1} assigned to a W−O_c−W antisymmetric stretching mode shows up. So, POM-2a should not align randomly but instead should have a particular orientation within the solvent-casting films of SEC-2. IR bands of POMs are difficult to assign exactly because of the extensive overlap of different bands, except that of the W−O_d antisymmetric stretching mode.[28] Therefore, one cannot precisely determine the orientation of POM-2a within the solvent-casting films by the IR linear dichromism technique. However, these results demonstrate that POM-2a in SEC-2 is organized by the simple solvent-casting technique.

X-ray diffraction pattern of the solvent-casting films of SEC-2 is shown in Figure 2B. One can discern three Bragg diffraction peaks at 2.46, 4.96, and 7.48°, corresponding to Bragg spacings of 3.6, 1.8, and 1.2 nm, respectively. The ratio of these three spacings suggests that the signals arise from a lamellar structure with a layer distance of 3.6 nm, which is consistent with the short periodicity of the solid-state SEC-2. Our present and previous results[14] show that the spacings are independent of the used concentrations of SEC-2 (0.05−2.5 mg/mL). Combining the length and the tilt angle of DODA alkyl chain, as well as the short-axis diameter of POM-2a cluster, the calculated monolayer thickness of the encapsulated structure is 4.9 nm, which is larger than the layer distance obtained by the X-ray diffraction. Herein, the partially interdigitated alkyl chains are considered in the solvent-casting films of SEC-2, and the interdigitated length is 1.3 nm (Figure 1B). The interdigitated structure is expected to be energetically favorable because of the resulting maximization of the hydrophobic interaction.[14,33,34] In contrast to the solid structure of SEC-2, this process should be primarily governed by the kinetic effect during the organic solvent evaporation. An AFM image of the samples offers a homogeneous surface with an aggregated texture, and its root-mean-square (RMS) value of the surface roughness is 0.35.

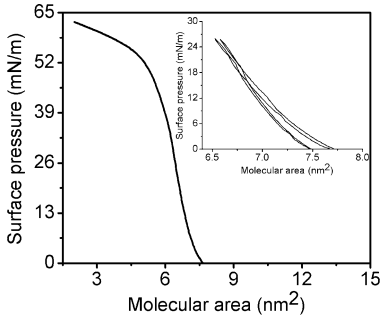

Figure 4. Surface pressure−area (π−A) isotherm of SEC-2 at the temperature of 18 °C. Inset: compression−expansion cycle π−A isotherm of SEC-2.

Langmuir−Blodgett Films. Langmuir technique offers a facile and elegant strategy to fabricate the well-ordered organic/inorganic superlattices for SECs at the air/water interface.[35,36] Figure 4 shows a reproducible surface pressure−area (π−A) isotherm of SEC-2 on the subphase of pure water, which is continuous and shows no distinct phase transition. The Langmuir monolayer demonstrates a typical condensed state and has a high collapse surface pressure of 55 mN/m, exhibiting a stable monolayer. Upon expansion, a slight hysteresis is observed (Figure 4, inset), which is attributed to the aggregation tendency of SEC-2. The second compression−expansion cycle gives almost identical results. The molecular area of SEC-2 was 4.8 nm^2 at the collapse point, which corresponds to the densest possible packing. DODA·Br possesses a volume of 1.03 nm^3 on the basis of its crystal structure.[29] Eleven DODA molecules occupy a volume of 11.33 nm^3. POM-2a, consisting of two lacunary Keggin structures linked by one Eu^{3+}, occupies a volume of approximately 1.18 nm^3. Therefore, the total volume of SEC-2 is estimated to be 12.51 nm^3, which corresponds to an ideal sphere with a diameter of 2.88 nm. This value is smaller than the translation distances obtained by the powdered X-ray diffraction of SEC-2. With this diameter, the molecular area is estimated to be approximately 6.51 nm^2, larger than the collapse area obtained from the Langmuir isotherm of SEC-2. Here, we propose that SEC-2 is distorted strongly at the air/water interface, and DODAs are partially dissociated from POM-2a.[15] Another possible bilayer model consists of a separate surfactant monolayer in contact with a diffuse layer of POM-2a in the aqueous subphase. In this case, the collapse area of 4.8 nm^2 would correspond to 11 surfactant molecules, that is, 0.44 nm^2 per DODA, which is smaller than that of DODA. Complete dissociation of DODAs from POM-2a leads to the geometric mismatch between DODAs and POM-2a in this Langmuir monolayers, where eleven surfactant molecules occupy an area of 4.8 nm^2, while POM-2a has a crossover area of only 1.70 nm^2. This means that almost 64% of DODA monolayers should have no charge-balancing counterions. Therefore, we prefer the partial dissociation of DODAs from POM-2a. The strong distortion of SEC-2 at the air/water interface can be attributed to being in a confined state, that is, the unfavorable energy when the hydrophobic SEC-2 was spread onto the water subphase.

The Langmuir monolayers are readily transferred onto solid substrates with a transfer ratio near 1. In the FT-IR transmission spectrum of multilayer LB films of SEC-2, the CH_2 stretching bands appear at 2918 and 2850 cm^{-1}, suggesting that DODA

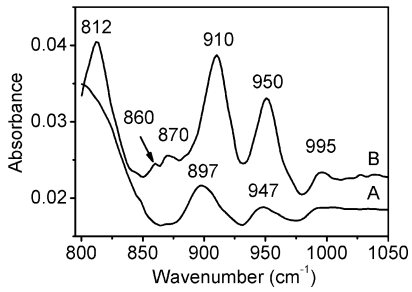

Figure 5. Transmission FT-IRspectrum (A), and reflection−absorption IR spectrum (B) of seventeen-layers LB films of SEC-2 deposited on CaF_2 and gold plates, respectively.

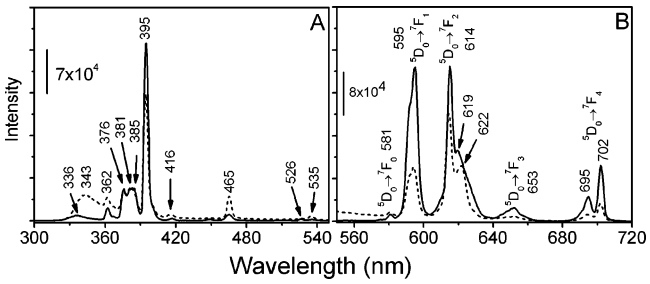

Figure 6. The excitation spectra (A) and the emission spectra (B) of POM-2 (full line) and SEC-2 (dashed line) solution with the concentrations of 1 mM at room temperature, respectively.

alkyl chains are well-ordered (Table 1). On the other hand, the full width at half-maximum (fwhm) of the CH_2 antisymmetric stretching absorption band is another measure of the conformational order of alkyl chains in ultrathin films, where an organized close-packed monolayer gives an fwhm of 17 cm^{-1} and a disordered ultrathin film can cause an fwhm greater than 35 cm^{-1}.[26,27,37] An fwhm of 16 cm^{-1} of the CH_2 antisymmetric stretching band in the LB film of SEC-2 indicates a crystal-like organization of the DODA alkyl chains. The linear increase of the IR absorbance with increase of the number of layers strongly suggests that the LB film growth is a uniform process.

According to the linear dichromism of the bands associated with the alkyl chains, the mean tilt angle of the alkyl chains is calculated to be about 31°. The linear dichromic ratios concerning the IR absorption bands of POM-2a also suggest that POM-2a is of both significant in-plane and out-of-plane anisotropies in the LB film of SEC-2 (Table 2). When the polarized angle is 90° and the incident angle is 0°, a new band appears at 812 cm^{-1}. These results indicate that POM-2a is of some oriented alignments in the LB film of SEC-2. More information about the organization of POM-2a in the LB films comes from the IR−RA spectrum. In contrast to the transmission spectrum of the LB film of SEC-2, its IR−RA spectrum shows the following varieties (Figure 5). Two strong bands at 812 and 910 cm^{-1} are assigned to W−O_c−W and Si−O_a antisymmetric stretching modes, respectively. Two weak bands at 860 and 870 cm^{-1} are attributed to a W−O_b−W antisymmetric stretching mode. A band at 897 cm^{-1} due to a W−O_b−W antisymmetric stretching mode disappears. The intensity of the band at 947 cm^{-1} due to a W−O_d antisymmetric stretching mode is much stronger in the RA spectrum than in the transmission spectrum. The W−O_d antisymmetric stretching mode is almost pure and offers a relatively sharp band,[28] which is more suitable for the comparison between the IR−RA and IR transmission spectra than other W−O stretching modes. According to the surface selection rule in IR−RA spectroscopy, vibrational modes with their transition moments perpendicular to surface are enhanced in an IR−RA spectrum.[38,39] The sharp contrast of the W−O_d antisymmetric stretching mode between the transmission and RA spectra suggests that the transition moment of the W−O_d antisymmetric stretching band should be perpendicular to the substrate. The W−O_d bond is vertical to the long axis of POM-2a on the basis of its structure. Therefore, the long axis orientation of POM-2a seems parallel to the substrate. This result can be further supported by X-ray diffraction of the LB film of SEC-2. In these results, the IR band positions in the reflection spectrum do not always correlate with the transmission spectrum. This may be because the anomalous dispersion of the sample layer contributes significantly to the reflectance of the sample−substrate interface in the RA spectrum, but these optical effects are absent in the transmission spectrum.[15,40]

The X-ray diffraction pattern of a nineteen-layer LB film of SEC-2 provides three Bragg peaks, as shown in Figure 2C. The three peaks can be clearly assigned to (001), (002), and (003) diffraction peaks, indicating that the layer structure of the LB films of SEC-2 is highly defined. The periodicity is calculated to be 4.9 nm, which is consistent with the long periodicity of the solid-state SEC-2. The long axis orientation of POM-2a was believed to be parallel to the substrate on the basis of the comparison between the IR−RA and transmission spectra. Combining the diameter of the short axis of POM-2a, the mean tilt angle, and the length of a DODA alkyl chain in the LB films of SEC-2, the total layer thickness can be estimated to be about 4.9 nm, consistent with the experimental value. This is quite different from the solvent-casting film of SEC-2 because the Langmuir monolayer packs closely as a confined state at the air/water interface and is transferred onto the substrates, but the former undergoes a kenetic process for the interdigitated DODA alkyl chains. Similar differences between LB and solvent-casting films are also observed for the amphiphilic polymers and results in their different thermal behaviors.[34,41] Herein, the structural differences between LB and casting films of SEC-2 cause their different photophysical properties.

Photophysical Properties. The excitation spectra of the solutions (1mM, POM-2 in water and SEC-2 in chloroform) at room temperature exhibit sharp lines, corresponding to the characteristic transitions with 4f^6 shell of Eu^{3+}, as shown in Figure 6A. The detailed assignments are as follows: 362 nm ($^7F_0 \rightarrow {}^5D_4$), 376 nm ($^7F_0 \rightarrow {}^5G_4$), 381 nm ($^7F_0 \rightarrow {}^5G_3$), 385 nm ($^7F_0 \rightarrow {}^5G_2$), 395 nm ($^7F_0 \rightarrow {}^5L_6$), 416 nm ($^7F_0 \rightarrow {}^5D_3$), 465 nm ($^7F_0 \rightarrow {}^5D_2$), 526 nm ($^7F_0 \rightarrow {}^5D_1$), and 535 nm ($^7F_1 \rightarrow {}^5D_1$).[8,9] The excitation intensity of the $^7F_0 \rightarrow {}^5L_6$ peak of the solution of SEC-2 is weaker than that of the solution of POM-2. In contrast, the peaks due to $^7F_0 \rightarrow {}^5D_2$ and $^7F_1 \rightarrow {}^5D_1$ are enhanced significantly in the solution of SEC-2. This should be ascribed to the different environments of POM-2a. A broad band at 336 nm is attributed to the O→W LMCT transition of the solution of POM-2. Of difference is that the LMCT band for the solution of SEC-2 appears at 343 nm and its intensity is much stronger than that for POM-2 aqueous solution. Therefore, it can be inferred that the energy transfer from the O→W LMCT states to Eu^{3+} ions is more efficient and the communication between the O→W LMCT and excited Eu^{3+} levels is drastically increased in SEC-2 solution.

The excitation spectrum of the solid-state SEC-2also shows the characteristic transitions with 4f^6 shell of Eu^{3+}, while the relative intensity of the O→W LMCT band (342 nm) compared with the $^7F_0 \rightarrow {}^5L_6$ peaks becomes pretty low (Figure 7A). The strong O→W LMCT bands for the solvent-casting and LB films appear at 316 and 291 nm, respectively, as shown in Figure 7A. This is due to their different layer structures. However, their characteristic transitions with 4f^6 shell of Eu^{3+} are very weak,

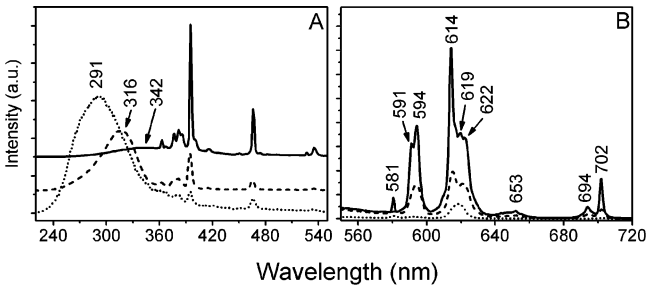

Figure 7. The excitation spectra (A) and the emission spectra (B) of the solid-state (full line), solvent-casting films (dashed line), and LB films (dotted line) of SEC-2, respectively.

TABLE 3: The Summary of the O→W LMCT Bands, Measured Intensity Ratios $I(^5D_0 \rightarrow {}^7F_2)/I(^5D_0 \rightarrow {}^7F_1)$, Luminescent Lifetimes, and Number of Coordinated Water Molecules for POM-2A in the Different States at Room Temperature

	LMCT band	$I(^5D_0 \rightarrow {}^7F_2)/I(^5D_0 \rightarrow {}^7F_1)$	lifetime (ms)	q [a]
SEC-2, solid state	341	2.5	0.844, 0.194	0.9, 5.0
SEC-2, solution	343	2.69	0.739	1
SEC-2, casting film	316	2.42	0.573	1.5
SEC-2, LB film	291	13.93	0.176	5.3
POM-2, solution (water)	336	1.23	3.3[c]	0
POM-2, solid state[c]		1.13	2.4	0
DODA/POM-2, LB films[d]	285	7.25	0.375	2.4
ODA[b]/POM-2, LB films[d]	290	1.55	0.482	1.8

[a] q, number of coordinated water molecules. [b] Octadecylamine. [c] Reference 19. [d] Reference 8.

significantly different from those of the solution and solid-state of SEC-2. These differences should result from their different organizational structures. LB films fabricated from surfactant monolayers on aqueous subphase containing POM-2 also offer similar strong charge-transfer bands.[8,9]

The emission spectra of POM-2 and SEC-2 solution with a concentration of 1 mM show the characteristic Eu^{3+} emission when excited at 395 nm (Figure 6B). The peaks are assigned to the $^5D_0 \rightarrow {}^7F_j$ ($j = 0-4$) transitions.[18,19] The intensities of the emissive bands of SEC-2 solution are lower than that those of the emissive bands of POM-2 solution, because of the different chemical microenvironments of POM-2a. The solid-state emission spectrum of SEC-2 shows more splits, for instance, $^5D_0 \rightarrow {}^7F_1$, 591 and 594 nm, $^5D_0 \rightarrow {}^7F_2$, 614, 619, and 622 nm (Figure 7B). The photoexcitations at the O→W LMCT bands of the solvent-casting and LB films of SEC-2 result in an efficient intramolecular energy transfer from the heteropolyoxotungatate to Eu^{3+}, and their emission spectra show the characteristic $^5D_0 \rightarrow {}^7F_j$ ($j = 0-4$) transitions of Eu^{3+} (Figure 7B). The $^5D_0 \rightarrow {}^7F_2$ transition is attributed to an electric dipole transition and is extremely sensitive to the chemical surroundings in the vicinity of Eu^{3+} ions. The intensity increases as the Eu−O covalency increases and environments become more symmetrical. On the other hand, the $^5D_0 \rightarrow {}^7F_1$ transition is a magnetic dipole transition, and its intensity is almost independent of the changes of Eu^{3+}'s chemical microenvironments. Therefore, the intensity ratio of the $^5D_0 \rightarrow {}^7F_2$ transition to the $^5D_0 \rightarrow {}^7F_1$ transition, as referred $I(^5D_0 \rightarrow {}^7F_2)/I(^5D_0 \rightarrow {}^7F_1)$, is widely used to study the chemical microenvironments of Eu^{3+} ions.[42,43] The relative data are summarized in Table 3. The intensity ratios of SEC-2 are larger than those of the naked POM-2, indicating that the encapsulation for POM-2a strongly affects the local environments of Eu^{3+} ions. The special large intensity ratio (13.93) of the LB film of SEC-2 may be due to the high symmetrical environments of POM-2a. Different intensity ratios, $I(^5D_0 \rightarrow {}^7F_2)/I(^5D_0 \rightarrow {}^7F_1)$, should be ascribed to different chemical environments, for example, the solid state, solution, solvent-casting film, and LB film of SEC-2. Our results are also different from those of LB films through adsorption of POM-2 in aqueous subphase by surfactant monolayers (Table 3), which may be due to their different structures.

The fluorescent lifetimes for the solid state, solution, solvent-casting film, and LB film of SEC-2 are summarized in Table 3. The solid-state SEC-2 shows a double-exponential decay (0.84 and 0.19 ms), corresponding to the two different structures and consistent with its X-ray diffraction data. Of difference is that the solvent-casting and LB films demonstrate single-exponential decays with the lifetimes of 0.57 and 0.18, respectively. The latter is in excellent agreement with the short lifetime for the solid-state SEC-2, which may be due to the similar chemical microenvironments for POM-2a. This is supported by their X-ray diffraction patterns that show identical spacings. The lifetime of the solvent-casting film is slightly smaller than the long lifetime of the solid-state SEC-2. These results also differ from those of LB films constructed from Langmuir monolayers adsorbing POM-2 in aqueous subphase[8,9] (see Table 3). Here, it is proposed that the POM-based LB films fabricated by SECs are structurally different from those prepared through adsorption of various polyoxometalates in aqueous subphase by DODA monolayers.

The lifetimes of SEC-2 at its various states are much shorter than those of the naked POM-2. Similar phenomena are also observed in LB films constructed from Langmuir monolayers adsorbing POM-2 in aqueous subphase.[8] Replacement of OH oscillators by OD makes the vibronic deexcitation pathway exceedingly inefficient.[21] SEC-2 prepared according to the procedures described in the experimental part except that POM-2 is dissolved in D_2O gives a double-exponential decay (2.85 and 0.471 ms). Therefore, in our case, the shortened lifetimes should be due to the coordinated water to Eu^{3+}. The number of water molecules coordinated to Eu^{3+} (q) can be calculated with an estimated uncertainty of 0.5, according to the following equation: $q = 1.05(1/\tau H_2O - 1/\tau D_2O)$, where τH_2O and τD_2O are the experimental excited-state lifetimes in H_2O and D_2O environments, respectively.[21] The different existing states of SEC-2 offer the different numbers of water molecules coordinated to the Eu^{3+} ion (see Table 3). The number of coordinated water molecules in the proposed formula of SEC-2 is within the range of the estimated values by the equation.

The solution, solid state, solvent-casting films, and LB films display different photophysical properties such as luminescence (containing excitation and emission spectra), lifetime, and energy transfer. Similar phenomena have been also observed in Eu^{3+} and Tb^{3+} complexes.[44−46] The unexpected photophysical properties are induced in the thin films of SEC-2, which are highly interesting and very important for the device realization; however, at present, a precise interpretation cannot be given because of the complexity of thin film systems. Also, there are several possible reasons for the different photophysical behaviors in thin films such as the lateral electron transfer, thermal diffusion, and the formation of a natural optical microcavity (the interface between quartz and thin film or thin film and air is believed to be a mirror due to the different refractive indexes).[44,45] The photophysical properties can be easily changed by modifying the surface chemical properties of POM-2 with positive charged surfactants. The electronic properties of SEC-2 come from POMs. However, the organic amphiphilic cation not only plays a structural role but also has a strong effect on photophysical behavior. In fact, metal cations such as Rb^+,

K^+, and Na^+ can coordinate on to POMs except for tetraalkylammoniums and Li^+.[47] In our case, the variations of the photophysical properties of POM-2a should originate from its counterion exchange with DODA.

Conclusions

In this article, we successively synthesized and characterized the surfactant-encapsulated europium-substituted heteropolyoxotungatate, $(DODA)_{11}H_2[Eu(SiW_{11}O_{39})_2(H_2O)_4]$ (SEC-2). This material exhibits the characteristic $^5D_0 \rightarrow {}^7F_j$ ($j = 0-4$) Eu^{3+} emission, and its photophysical properties such as excited, emissive spectra, lifetime, and energy transfer from the O→W LMCT state to Eu^{3+} ion are significantly different from those of POM-2 (see Table 3). Although the electronic properties of SEC-2 originate from POM-2a, the cationic surfactant plays an important role in modifying its photophysical behaviors. However, the precise mechanism concerning the changes of electronic configurations of POM-2a is not clear. The photophysical properties of europium-substituted polyoxometalates (Eu−POMs) can be easily modified by improvement of their surface chemical properties. Further studies will focus on the electronic properties of POMs before and after the encapsulation with cationic surfactants.

The solution, solid state, solvent-casting films, and LB films of SEC-2 show different photophysical behaviors (Table 3), which is attributed to their different packing structures. Of significance is that the photophysical properties of SEC-2 in its thin films can be modified by careful change of the lamellar distance in the different organized thin films, for example, LB and solvent-casting films. The two packing structures of the solid-state SEC-2 correspond to those of the LB and casting films of SEC-2, respectively (Figure 1 and Figure 2). Consequently, the long and short lifetimes of the solid-state SEC-2 are similar to those of the casting and LB films of SEC-2, respectively. Here, we offer a model study for the controllable relationship between the nanostructures and properties of functional POMs. We also compared the photophysical behaviors between the POM-based LB films fabricated by SEC-2 and those through adsorption of POM-2 in the aqueous subphase by DODA monolayers. On the basis of their different photophysical behaviors, the two kinds of LB films should possess different packing structures. These results are significant for the functional realization of POMs.

Acknowledgment. This work is supported from the Key Project of National Natural Science Foundation of China (29992590-5), the Major State Basic Research Development Program (G200078102), and the Ministry of Education, China. The authors thank Mr. Hongyu Zhang for his helpful discussion in the synthesis of $K_{13}Eu(SiW_{11}O_{39})_2 \cdot 20H_2O$, and Professor Yuqing Wu and Ms. Chunxi Zhai for the fitting of the decay curves. We appreciate Mr. Tao Wu from Princeton University, Mr. Steve Lenhert from the University of Münster, and Professor Adam Baszkin for their kind assistance of English.

References and Notes

(1) Kunitake, T. In *Synthetic Bilayer Membranes*: *Molecular Design and Molecular Organization, Comprehensive Supramolecular Chemistry;* Atwood, J. L., Davies, J. E. D., MacNicol, D. D., Vögle, F., Lehn, J.-M., Sauvage, J.-P., Hosseini, M. W., Eds.; Pergamon: Oxford, 1996; Vol. 9.
(2) Fendler, J. H.; Meldrum, F. C. *Adv. Mater*. **1995**, *7*, 607.
(3) Wang, E. B.; Hu, C. W.; Xu, L. *Introduction to polyoxometalate Chemistry*; Chemical Industry Press: Beijing, 1998.
(4) *Chem. Rev*. **1998**, 98, 1. The entire issue is devoted to polyoxometalates.
(5) Chemente-León, M.; Agricole, B.; Mingotaud, C.; Gómez-García, C. J.; Coronado, E.; Delhaes, P. *Langmuir* **1997**, *13*, 2340.
(6) Chemente-León, M.; Agricole, B.; Mingotaud, C.; Gómez-García, C. J.; Coronado, E.; Delhaes, P. *Angew. Chem. Int. Ed. Engl*. **1997**, *36*, 1114.
(7) Coronado, E.; Mingotaud, C. *Adv. Mater*. **1999**, *11*, 869.
(8) Wang, J.; Wang, H. S.; Fu, L. S.; Liu, F. Y.; Zhang, H. J. *Thin Solid Films* **2002**, *414*, 256.
(9) Wang, J.; Wang, H. S.; Liu, F. Y.; Fu, L. S.; Zhang, H. J. *J. Lumin*. **2003**, *101*, 63.
(10) Polarz, S.; Smarsly, B.; Antonietti, M. *Chem. Phys. Chem.* **2001**, *1*, 457.
(11) Kurth, D. G.; Lehmann, P.; Volkmer, D.; Cölfen, H.; Koop, M. J.; Müller, A.; Du Chesne, A. *Chem. Eur. J*. **2000**, *6*, 385.
(12) Volkmer, D.; Du Chesne, A.; Kurth, D. G.; Schnablegger, H.; Lehmann, P.; Koop, M. J.; Müller, A. *J. Am. Chem. Soc*. **2000**, *122*, 1995.
(13) Kurth, D. G.; Lehmann, P.; Volkmer, D.; Müller, A.; Schwahn, D. *J. Chem. Soc., Dalton Trans*. **2000**, 3989.
(14) Bu, W.; Wu, L.; Hou, X.; Fan, H.; Hu, C.; Zhang, X. *J. Colloid Interface Sci*. **2002**, *251*, 120.
(15) Bu, W.; Fan, H.; Wu, L.; Hou, X.; Hu, C.; Zhang, G.; Zhang, X. *Langmuir* **2002**, *18*, 6398.
(16) Bu, W.; Zhang, J.; Wu, L.; Tang, A. C. *Chin. J. Chem*. **2002**, *20*, 1514.
(17) Volkmer, D.; Bredenkötter, B.; Tellenbröker, J.; Kögerler, P.; Kurth, D. G.; Lehmann, P.; Schnablegger, H.; Schwahn, D.; Piepenbrink, M.; Krebs, B. *J. Am. Chem. Soc*. **2002**, *124*, 10489.
(18) Blasse, G.; Dirksen, G. J.; Zonnevijlle, F. *J. Inorg. Nucl. Chem*. **1981**, *43*, 2847.
(19) Ballardini, R.; Chiorboli, E.; Balzani, V. *Inorg. Chim. Acta* **1984**, *95*, 323.
(20) Tourné, C. M.; Tourné, G. F.; Brianso, M. C. *Acta Cryst*. **1980**, *B36*, 2012.
(21) Horrocks, W. D., Jr.; Sudnick, D. R. *Acc. Chem. Res.* **1981**, *14*, 384.
(22) Peacock, R. D.; Weakley, T. J. R. *J. Chem. Soc. A* **1971**, 1836.
(23) Wassermann, K.; Pope, M. T. *Inorg. Chem*. **2001**, *40*, 2763.
(24) Umemura, J.; Cameron, D. G.; Mantsch, H. H. *Biochim. Biophys. Acta* **1980**, *602*, 32.
(25) Sapper, H.; Cameron, D. G.; Mantsch, H. H. *Can. J. Chem*. **1981**, *59*, 2543.
(26) Maoz, R.; Sagiv, J. *J. Colloid Interface Sci*. **1984**, *100*, 465.
(27) Porter, M. D.; Bright, T. B.; Allara, D. L.; Chidsey, C. E. D. *J. Am. Chem. Soc*. **1987**, *109*, 3559.
(28) Rocchoccioli-Deltcheff, C.; Fournier, M.; Franck, R.; Thouvenot, R. *Inorg. Chem*. **1983**, *22*, 207.
(29) Okuyama K.; Soboi Y.; Iijima N.; Hirabayashi K.; Kunitake T.; Kajiyama T. *Bull. Chem. Soc. Jpn*. **1988**, *61*, 1485.
(30) Myrzakozha, D. A.; Hasegawa, T.; Nishijo, J.; Imae, T.; Ozaki, Y. *Langmuir* **1999**, *15*, 6890.
(31) Myrzakozha, D. A.; Hasegawa, T.; Nishijo, J.; Imae, T.; Ozaki, Y. *Langmuir* **1999**, *15*, 3601.
(32) Vandevyver, M.; Barrau, A.; Raudel-Teixier, A.; Maillard, P.; Gianotti, C. *J. Colloid Interface Sci*. **1982**, *85*, 571.
(33) Israelachili, J. N. *Intermolecular and Surface Force*, 2nd ed.; Academic Press: New York, 1991.
(34) Zhang, X.; Li, H.; Zhao, B.; Shen, J.; Gao, Z.; Li, X. *Macromolecules* **1997**, *30*, 1633.
(35) Petty, M. C. *Langmuir-Blodgette Films An Introduction*; Cambridge Press: 1996.
(36) Ulmann, A. *An Introduction to Ultrathin Organic Films from Langmuir-Blodgett to Self-Assembly*; Academic Press: New York, 1991.
(37) Seip, C. T.; Granroth, G. E.; Meisel, M. W.; Talham, D. R. *J. Am. Chem. Soc*. **1997**, *119*, 7084.
(38) Greenler, R. G. *J. Chem. Phys*. **1966**, *44*, 310.
(39) Chollet, P. A.; Messier, J.; Rosilio, C. *J. Chem. Phys*. **1976**, *64*, 1042.
(40) Kurth, D. G.; Bein, T. *Langmuir* **1995**, *11*, 578.
(41) Zhao, B.; Li, H.; Zhang, X.; Shen, J.; Ozaki, Y. *J. Phys. Chem. B* **1998**, *102*, 6515.
(42) Nogami, M.; Abe, Y. *J. Non-Cryst. Solids* **1996**, *197*, 73.
(43) Capobianco, J. A.; Proulx, P. P.; Bettinelli, M.; Negrisolo, F. *Phys. Rev. B* **1990**, *42*, 5936.
(44) Zhou, D.; Huang, C. H.; Yao, G.; Bai, J.; Li, T. K. *J. Alloys Comp*. **1996**, *235*, 156.
(45) Zhao, Y.; Zhou, D.; Yao, G.; Huang, C. H. *Langmuir* **1997**, *13*, 4060.
(46) Hazenkamp, M. F.; Blasse, G.; Sabbatini, N. *J. Phys. Chem*. **1991**, *95*, 783.
(47) Kirby, J. F.; Baker, L. C. W. *Inorg. Chem*. **1998**, *37*, 5537.